MULTIDIMENSIONAL UNITARY TENSOR-ESPRIT FOR NON-CIRCULAR SOURCES

Florian Roemer and Martin Haardt

Ilmenau University of Technology, Communications Research Laboratory
P.O. Box 100565, D-98684 Ilmenau, Germany, http://tu-ilmenau.de/crl
florian.roemer@ieee.org, haardt@ieee.org

***Abstract* — Recently, many authors have shown that high-resolution parameter estimation schemes can be significantly improved if the sources are non-circular. For example, enhanced versions of Root MUSIC and standard ESPRIT for non-circular sources as well as the entirely real-valued NC Unitary ESPRIT algorithm have been proposed.**

We can achieve further enhancements in the R-dimensional (R-D) case by using tensor algebra to express and manipulate multidimensional signals in their natural R-D structure. This has led to tensor-based parameter estimation algorithms with enhanced estimation accuracy such as R-D Unitary Tensor-ESPRIT.

In this paper we demonstrate how to achieve both benefits at the same time. This is not straightforward since the usual method to exploit non-circular sources destroys the tensor structure and therefore a new approach had to be found. This approach allows us to derive the NC R-D Unitary Tensor-ESPRIT algorithm which exploits the non-circularity of the sources and the R-D structure of the measured signals jointly. Numerical computer simulations demonstrate the benefit in terms of a significantly improved accuracy compared to state of the art algorithms.

Index Terms— Multidimensional signal processing, Parameter estimation, Array signal processing, Direction of arrival estimation

1. INTRODUCTION

Multi-dimensional harmonic retrieval problems are encountered in a variety of signal processing applications including radar, sonar, communications, medical imaging, and the estimation of the parameters of the dominant multipath components from MIMO channel measurements. R-dimensional subspace-based methods such as R-D Unitary ESPRIT, R-D MUSIC, or R-D RARE, have become popular solutions for this task.

One recent source of improvement of these methods has come from the use of tensors which allow a more flexible treatment of R-dimensional signals. For example, in [8] R-D Unitary Tensor-ESPRIT was derived and it was shown that tensor-based improved subspace estimates can enhance any subspace-based R-D parameter estimation scheme.

Recent investigations have also shown that the accuracy of harmonic retrieval algorithms can be significantly enhanced if the sources transmit non-circular symbols [3]. Corresponding versions of Root MUSIC, 2-D Root MUSIC standard ESPRIT, and R-D Unitary ESPRIT are discussed in [1], [11], [13], and [7], respectively.

In this paper we demonstrate how we can exploit the tensor structure of the R-D data model and non-circular source signals at the same time. This is not straightforward since the usual way to take advantage of non-circular source signals is to define an augmented measurement matrix with twice the number of sensors. However, this augmentation destroys the R-D structure of the measurements and thus the augmented measurement matrix cannot be written in tensor form any more.

We therefore derive a novel way to exploit non-circular sources using tensors. This is achieved by defining augmentations in all dimensions and then combining these through a modified version of the tensor shift invariance equations. This leads to the NC R-D Unitary Tensor-ESPRIT algorithm that captures the benefits of NC Unitary ESPRIT [7] and R-D Unitary Tensor-ESPRIT [8] at the same time. We also demonstrate the enhanced accuracy via computer simulations and compare the performance of the algorithms to the corresponding Cramér-Rao bounds (cf. [9]).

2. NOTATION

To distinguish between scalars, vectors, matrices, and tensors, the following notation is used throughout the paper: Scalars are denoted as italic letters (a, b, A, B), vectors as lower-case bold-faced letters ($\boldsymbol{a}, \boldsymbol{b}$), matrices are represented by upper-case bold-faced letters ($\boldsymbol{A}, \boldsymbol{B}$), and tensors are written as bold-faced calligraphic letters ($\boldsymbol{\mathcal{A}}, \boldsymbol{\mathcal{B}}$).

The superscripts ${}^{\mathrm{T}}, {}^{\mathrm{H}}, {}^{-1}$ represent (matrix) transposition, Hermitian transposition, and matrix inversion, respectively. Moreover, * denotes the complex conjugate operator.

An R-dimensional tensor $\boldsymbol{\mathcal{A}} \in \mathbb{C}^{M_1 \times M_2 \ldots \times M_R}$ is an R-way array of size M_r along mode r. The r-mode vectors of $\boldsymbol{\mathcal{A}}$ are obtained by varying the r-th index and keeping all other indices fixed. Collecting all r-mode vectors into a matrix we obtain the r-mode unfolding of $\boldsymbol{\mathcal{A}}$ which is represented by $[\boldsymbol{\mathcal{A}}]_{(r)} \in \mathbb{C}^{M_r \times M_{r+1} \cdot \ldots \cdot M_R \cdot M_1 \cdot \ldots \cdot M_{r-1}}$. The ordering of the columns in $[\boldsymbol{\mathcal{A}}]_{(r)}$ is chosen in accordance with [2]. The r-rank of $\boldsymbol{\mathcal{A}}$ is defined as the rank of $[\boldsymbol{\mathcal{A}}]_{(r)}$. Note that in general, all the r-ranks of a tensor $\boldsymbol{\mathcal{A}}$ can be different.

The r-mode product between a tensor $\boldsymbol{\mathcal{A}} \in \mathbb{C}^{M_1 \times M_2 \ldots \times M_R}$ and a matrix $\boldsymbol{U}_r \in \mathbb{C}^{P_r \times M_r}$ is symbolized by $\boldsymbol{\mathcal{B}} = \boldsymbol{\mathcal{A}} \times_r \boldsymbol{U}_r$. It is computed by multiplying all r-mode vectors from the left-hand side by the matrix $\boldsymbol{U}_r$, i.e., $[\boldsymbol{\mathcal{B}}]_{(r)} = \boldsymbol{U}_r \cdot [\boldsymbol{\mathcal{A}}]_{(r)}$.

The Higher-Order SVD (HOSVD) of a tensor $\boldsymbol{\mathcal{A}} \in \mathbb{C}^{M_1 \times M_2 \ldots \times M_R}$ is given by

$$\boldsymbol{\mathcal{A}} = \boldsymbol{\mathcal{S}} \times_1 \boldsymbol{U}_1 \times_2 \boldsymbol{U}_2 \ldots \times_R \boldsymbol{U}_R$$

where $\boldsymbol{\mathcal{S}} \in \mathbb{C}^{M_1 \times M_2 \ldots \times M_R}$ is the core tensor, which satisfies the all-orthogonality conditions [2] and $\boldsymbol{U}_r \in \mathbb{C}^{M_R \times M_R}$ are the unitary matrices of r-mode singular vectors for $r = 1, 2, \ldots, R$.

To represent the concatenation of two tensor $\boldsymbol{\mathcal{A}}$ and $\boldsymbol{\mathcal{B}}$ along the r-th mode we use the operator $[\boldsymbol{\mathcal{A}} \sqcup_r \boldsymbol{\mathcal{B}}]$ [10]. Note that two tensors can only be concatenated along the r-th mode if they have the same size in all modes $q \neq r,\ q = 1, 2, \ldots, R$.

978-1-4244-2354-5/09/$25.00 ©2009 IEEE

3. DATA MODEL

In this paper we study R-dimensional harmonic retrieval problems for data sampled on an R-dimensional grid. The underlying data model for the observation of d sources using an R-dimensional array with $M_1 \times M_2 \ldots \times M_R$ sensors that collects N snapshots in time can be described in the following fashion [8]

$$\boldsymbol{\mathcal{X}} = \boldsymbol{\mathcal{A}} \times_{R+1} \boldsymbol{S}^{\mathrm{T}} + \boldsymbol{\mathcal{N}}. \tag{1}$$

Here, $\boldsymbol{\mathcal{A}} \in \mathbb{C}^{M_1 \times \ldots \times M_R \times d}$ represents the array steering tensor which depends on the unknown spatial frequencies $\mu_i^{(r)}$ for the i-th source in the r-th mode for $i = 1, 2, \ldots, d$ and $r = 1, 2, \ldots, R$. The tensor $\boldsymbol{\mathcal{N}} \in \mathbb{C}^{M_1 \times \ldots \times M_R \times N}$ consists of samples of the additive noise process at the receiver and the matrix $\boldsymbol{S} \in \mathbb{C}^{d \times N}$ contains the source symbols $s_i(t_n)$ for $i = 1, 2, \ldots, d$ and $n = 1, 2, \ldots, N$.

An equivalent matrix representation of (1) is given by

$$\boldsymbol{X} = \boldsymbol{A} \cdot \boldsymbol{S} + \boldsymbol{N}, \tag{2}$$

where $\boldsymbol{X} = [\boldsymbol{\mathcal{X}}]^{\mathrm{T}}_{(R+1)} \in \mathbb{C}^{M \times N}$, $\boldsymbol{A} = [\boldsymbol{\mathcal{A}}]^{\mathrm{T}}_{(R+1)} \in \mathbb{C}^{M \times d}$, and $\boldsymbol{N} = [\boldsymbol{\mathcal{N}}]^{\mathrm{T}}_{(R+1)} \in \mathbb{C}^{M \times N}$. Here we have used the short hand notation $M = M_1 \cdot M_2 \cdot \ldots \cdot M_R$ for the total number of sensors.

In order to use ESPRIT-type algorithms we require the array to have a shift-invariant structure in all R modes [6]. Additionally, for NC R-D Unitary Tensor-ESPRIT, we need an array that is centro-symmetric [5], i.e., $\boldsymbol{\Pi}_M \cdot \boldsymbol{A}^* = \boldsymbol{A} \cdot \boldsymbol{\Delta}$ for some unitary diagonal matrix $\boldsymbol{\Delta} \in \mathbb{C}^{d \times d}$, where $\boldsymbol{\Pi}_M$ is the $M \times M$ exchange matrix with ones on its antidiagonal and zeros elsewhere. In other words, the (m_1, m_2)-element of $\boldsymbol{\Pi}_M$ is equal to one if $m_1 + m_2 = M + 1$.

To apply the enhanced Tensor-ESPRIT-type algorithms for non-circular sources, we require each user to emit strict-sense non-circular signals [9]. This condition implies that the symbols are real-valued (e.g., BPSK, M-ASK[1]) except for an arbitrary phase angle φ_i, $i = 1, 2, \ldots, d$. We can include this assumption in the data model by factorizing the matrix $\boldsymbol{S}$ in the following way [7]

$$\boldsymbol{S} = \boldsymbol{\Psi} \cdot \boldsymbol{S}_0, \quad \text{where } \boldsymbol{S}_0 \in \mathbb{R}^{d \times N} \quad \text{and} \tag{3}$$

$$\boldsymbol{\Psi} = \operatorname{diag}\left\{ \left[e^{j\varphi_1}, e^{j\varphi_2}, \ldots, e^{j\varphi_d} \right] \right\}. \tag{4}$$

4. R-D SHIFT INVARIANCE

In this section we revisit the tensor-valued shift invariance equations from [8] and propose a modification on how to solve them which is useful in deriving the NC R-D Unitary Tensor-ESPRIT algorithm.

In order to apply R-D ESPRIT-type algorithms, the array must be shift invariant in R dimensions. This can be expressed in the following set of tensor equations

$$\boldsymbol{\mathcal{A}} \times_r \boldsymbol{J}_1^{(r)} \times_{R+1} \boldsymbol{\Phi}^{(r)} = \boldsymbol{\mathcal{A}} \times_r \boldsymbol{J}_2^{(r)}. \tag{5}$$

Here, $\boldsymbol{J}_1^{(r)}, \boldsymbol{J}_2^{(r)} \in \mathbb{R}^{M_r^{(\mathrm{sel})} \times M_r}$ represent the selection matrices that select $M_r^{(\mathrm{sel})}$ out of M_r sensors for the first and the second subarray in the r-th mode and $\boldsymbol{\Phi}^{(r)} = \operatorname{diag}\left\{ \left[e^{j\mu_1^{(r)}}, \ldots, e^{j\mu_d^{(r)}} \right] \right\}$.

In presence of d sources, all the n-ranks of the noise-free signal component in (1) are less than or equal to d. We can therefore compute an HOSVD-based low-rank approximation of $\boldsymbol{\mathcal{X}}$ in the following way

$$\boldsymbol{\mathcal{X}} \approx \boldsymbol{\mathcal{S}}^{[\mathrm{s}]} \times_1 \boldsymbol{U}_1^{[\mathrm{s}]} \ldots \times_R \boldsymbol{U}_R^{[\mathrm{s}]} \times_{R+1} \boldsymbol{U}_{R+1}^{[\mathrm{s}]} \quad \text{where} \tag{6}$$
$$\boldsymbol{\mathcal{S}}^{[\mathrm{s}]} \in \mathbb{C}^{p_1 \times p_2 \ldots \times d},$$
$$\boldsymbol{U}_r^{[\mathrm{s}]} \in \mathbb{C}^{M_r \times p_r} \text{ for } r = 1, 2, \ldots, R \quad \text{and } \boldsymbol{U}_{R+1}^{[\mathrm{s}]} \in \mathbb{C}^{N \times d}.$$

Here, $p_r = \min\{M_r, d\}$ for $r = 1, 2, \ldots, R$. The tensor $\boldsymbol{\mathcal{S}}^{[\mathrm{s}]}$ is obtained from the core tensor $\boldsymbol{\mathcal{S}}$ of the HOSVD of $\boldsymbol{\mathcal{X}}$ by truncating it to p_r elements in the r-th mode. Similarly, $\boldsymbol{U}_r^{[\mathrm{s}]}$ is obtained by truncating the r-mode singular vector matrix $\boldsymbol{U}_r$ to p_r columns. Note that we have assumed $N \geq d$. If N is smaller, preprocessing in the form of forward-backward averaging (which is always included in Unitary ESPRIT) and/or spatial smoothing can be applied to virtually increase the number of snapshots N. For simplicity, in the sequel we ignore the influence of the noise and write equalities. In the presence of noise, the following HOSVDs represent low-rank approximations and the shift invariance equations based on the estimated subspaces hold approximately (creating the need for an appropriate least squares method to solve them).

In [8] we have shown that the unknown array steering tensor $\boldsymbol{\mathcal{A}}$ in (5) can be eliminated using the HOSVD of $\boldsymbol{\mathcal{X}}$. We then obtain the shift invariance relations in the following form

$$\boldsymbol{\mathcal{U}}^{[\mathrm{s}]} \times_r \boldsymbol{J}_1^{(r)} \times_{R+1} \boldsymbol{\Psi}^{(r)} = \boldsymbol{\mathcal{U}}^{[\mathrm{s}]} \times_r \boldsymbol{J}_2^{(r)}, \tag{7}$$

which can be solved for the unknown matrices $\boldsymbol{\Psi}^{(r)}$ using an appropriate least squares technique (e.g., LS, SLS [4], or TS-SLS [10]). Here, we use the definition $\boldsymbol{\mathcal{U}}^{[\mathrm{s}]} = \boldsymbol{\mathcal{S}}^{[\mathrm{s}]} \times_1 \boldsymbol{U}_1^{[\mathrm{s}]} \ldots \times_R \boldsymbol{U}_R^{[\mathrm{s}]}$.

Alternatively, we can express (7) in the following equivalent form

$$\boldsymbol{\mathcal{V}}_r^{[\mathrm{s}]} \times_r \boldsymbol{J}_1^{(r)} \times_{R+1} \boldsymbol{\Psi}^{(r)} = \boldsymbol{\mathcal{V}}^{[\mathrm{s}]} \times_r \boldsymbol{J}_2^{(r)}, \tag{8}$$

where $\boldsymbol{\mathcal{V}}_r^{[\mathrm{s}]} = \boldsymbol{\mathcal{S}}^{[\mathrm{s}]} \times_r \boldsymbol{U}_r^{[\mathrm{s}]}$. This form of the shift invariance equations is easily derived from (7) by applying the q-mode product with $\boldsymbol{U}_q^{[\mathrm{s}]^{\mathrm{H}}}$ for all $q = 1, 2, \ldots, R$, $q \neq r$. It is worth noting that even though solving (7) or (8) yields exactly the same solution in $\boldsymbol{\Psi}^{(r)}$, for a small d the complexity of solving (8) is lower because $\boldsymbol{\mathcal{V}}_r^{[\mathrm{s}]}$ has less elements than $\boldsymbol{\mathcal{U}}^{[\mathrm{s}]}$.

In [8] we have also shown that forward-backward averaging can be applied to the measurement tensor and that this tensor can be transformed into an equivalent real-valued tensor of size $M_1 \times M_2 \ldots \times M_R \times 2N$. We then compute the real-valued HOSVD of the transformed measurement tensor $\varphi(\boldsymbol{\mathcal{X}})$ in the following fashion

$$\varphi(\boldsymbol{\mathcal{X}}) = \boldsymbol{\mathcal{L}}^{[\mathrm{s}]} \times_1 \boldsymbol{E}_1^{[\mathrm{s}]} \ldots \times_R \boldsymbol{E}_R^{[\mathrm{s}]} \times_{R+1} \boldsymbol{E}_{R+1}^{[\mathrm{s}]}. \tag{9}$$

The real-valued invariance equations can now also be stated in two forms

$$\boldsymbol{\mathcal{E}}^{[\mathrm{s}]} \times_r \boldsymbol{K}_1^{(r)} \times_{R+1} \boldsymbol{\Upsilon}^{(r)} = \boldsymbol{\mathcal{E}}^{[\mathrm{s}]} \times_r \boldsymbol{K}_2^{(r)} \tag{10}$$

$$\boldsymbol{\mathcal{F}}_r^{[\mathrm{s}]} \times_r \boldsymbol{K}_1^{(r)} \times_{R+1} \boldsymbol{\Upsilon}^{(r)} = \boldsymbol{\mathcal{F}}_r^{[\mathrm{s}]} \times_r \boldsymbol{K}_2^{(r)}, \tag{11}$$

where (10) was derived in [8] for $\boldsymbol{\mathcal{E}}^{[\mathrm{s}]} = \boldsymbol{\mathcal{L}}^{[\mathrm{s}]} \times_1 \boldsymbol{E}_1^{[\mathrm{s}]} \ldots \times_R \boldsymbol{E}_R^{[\mathrm{s}]}$ and (11) is the modified version with $\boldsymbol{\mathcal{F}}_r^{[\mathrm{s}]} = \boldsymbol{\mathcal{L}}^{[\mathrm{s}]} \times_r \boldsymbol{E}_r^{[\mathrm{s}]}$. Here $\boldsymbol{K}_{1,2}^{(r)}$ represent the transformed selection matrices (cf. [8]).

[1] Note that we can also include modulation schemes for which the phase is not constant but varies deterministically, e.g., MSK or OQPSK. These can be turned into real-valued constellations by proper derotation, i.e., a compensation of the deterministic phase at the receiver.

5. NC R-D UNITARY TENSOR-ESPRIT

In [7] we have shown that in the presence of strict sense non-circular sources we can virtually double the number of available sensors by defining the augmented measurement matrix $\boldsymbol{X}^{(\mathrm{nc})}$ in the following fashion

$$\boldsymbol{X}^{(\mathrm{nc})} = \begin{bmatrix} \boldsymbol{X} \\ \boldsymbol{\Pi} \cdot \boldsymbol{X}^* \end{bmatrix} \in \mathbb{C}^{2M \times N}, \tag{12}$$

which admits a factorization into

$$\boldsymbol{X}^{(\mathrm{nc})} = \boldsymbol{A}^{(\mathrm{nc})} \cdot \boldsymbol{S} + \boldsymbol{N}^{(\mathrm{nc})}, \quad \text{where} \tag{13}$$
$$\boldsymbol{A}^{(\mathrm{nc})} = \begin{bmatrix} \boldsymbol{A} \\ \boldsymbol{\Pi} \cdot \boldsymbol{A}^* \cdot \boldsymbol{\Psi}^* \cdot \boldsymbol{\Psi}^* \end{bmatrix} \text{ and } \boldsymbol{N}^{(\mathrm{nc})} = \begin{bmatrix} \boldsymbol{N} \\ \boldsymbol{\Pi} \cdot \boldsymbol{N}^* \end{bmatrix}.$$

Note that in (13) we have used the fact that $\boldsymbol{S}$ can be factored according to (3) if it contains strict sense non-circular sources. In the tensor case, we cannot apply the same operation since $\boldsymbol{X}^{(\mathrm{nc})}$ cannot be expressed in tensor form. However, the augmentation operation can be applied in any of the R modes. This leads to R different ways of defining an augmented measurement tensor

$$\boldsymbol{\mathcal{X}}^{(\mathrm{nc},r)} = \left[\boldsymbol{\mathcal{X}} \sqcup_r \tilde{\boldsymbol{\mathcal{X}}}\right] \text{ where} \tag{14}$$
$$\tilde{\boldsymbol{\mathcal{X}}} = \boldsymbol{\mathcal{X}}^* \times_1 \boldsymbol{\Pi}_{M_1} \ldots \times_R \boldsymbol{\Pi}_{M_R}.$$

Note that $\boldsymbol{\mathcal{X}}^{(\mathrm{nc},r)}$ has size $2M_r$ along mode r.

Let us introduce the HOSVD of $\boldsymbol{\mathcal{X}}^{(\mathrm{nc},r)}$ in the following fashion

$$\boldsymbol{\mathcal{X}}^{(\mathrm{nc},r)} = \boldsymbol{\mathcal{S}}^{(r)[\mathrm{s}]} \times_1 \boldsymbol{U}_1^{(r)[\mathrm{s}]} \ldots \times_R \boldsymbol{U}_R^{(r)[\mathrm{s}]} \times_{R+1} \boldsymbol{U}_{R+1}^{(r)[\mathrm{s}]}. \tag{15}$$

Note that for simplicity we ignore the influence of the noise as in the previous section and use the truncated HOSVD defined in [8]. From the R HOSVDs ($r = 1, 2, \ldots, R$) we can construct R shift invariance equations using the modified form defined in (8)

$$\boldsymbol{\mathcal{V}}_r^{(\mathrm{nc},r)} \times_r \boldsymbol{J}_1^{(\mathrm{nc})(r)} \times_{R+1} \boldsymbol{\Psi}^{(r)} = \boldsymbol{\mathcal{V}}_r^{(\mathrm{nc},r)} \times_r \boldsymbol{J}_2^{(\mathrm{nc})(r)}$$
$$\text{where } \boldsymbol{\mathcal{V}}_r^{(\mathrm{nc},r)} = \boldsymbol{\mathcal{S}}^{(r)[\mathrm{s}]} \times_r \boldsymbol{U}_r^{(r)[\mathrm{s}]}. \tag{16}$$

Here, $\boldsymbol{J}_n^{(\mathrm{nc})(r)} \in \mathbb{R}^{2M_r^{(\mathrm{sel})} \times 2M_r}$ represent the extended selection matrices that can be computed from $\boldsymbol{J}_n^{(r)}$ for $n = 1, 2$ and $r = 1, 2, \ldots, R$ in the following fashion

$$\boldsymbol{J}_1^{(\mathrm{nc})(r)} = \begin{bmatrix} \boldsymbol{J}_1^{(r)} & \boldsymbol{0}_{M_r^{(\mathrm{sel})} \times M_r} \\ \boldsymbol{0}_{M_r^{(\mathrm{sel})} \times M_r} & \boldsymbol{\Pi}_{M_r^{(\mathrm{sel})}} \cdot \boldsymbol{J}_2^{(r)} \cdot \boldsymbol{\Pi}_{M_r} \end{bmatrix} \tag{17}$$

$$\boldsymbol{J}_2^{(\mathrm{nc})(r)} = \begin{bmatrix} \boldsymbol{J}_2^{(r)} & \boldsymbol{0}_{M_r^{(\mathrm{sel})} \times M_r} \\ \boldsymbol{0}_{M_r^{(\mathrm{sel})} \times M_r} & \boldsymbol{\Pi}_{M_r^{(\mathrm{sel})}} \cdot \boldsymbol{J}_1^{(r)} \cdot \boldsymbol{\Pi}_{M_r} \end{bmatrix}. \tag{18}$$

Note that for centro-symmetric arrays, (17) and (18) simplify to $\boldsymbol{J}_n^{(\mathrm{nc})(r)} = \boldsymbol{I}_2 \otimes \boldsymbol{J}_n^{(r)}$ for $n = 1, 2$, since then $\boldsymbol{\Pi}_{M_r^{(\mathrm{sel})}} \cdot \boldsymbol{J}_1^{(r)} \cdot \boldsymbol{\Pi}_{M_r} = \boldsymbol{J}_2^{(r)}$ [6]. This shows that the number of sensors is virtually doubled for each of the shift invariance equations we solve.[2]

Due to the fact that we restricted our attention to centro-symmetric arrays, we can apply forward-backward averaging and then transform the shift invariance equations into the real-valued domain. Since the resulting method is a combination of NC Unitary ESPRIT [7] and R-D Unitary Tensor-ESPRIT [8] it will be termed NC R-D Unitary Tensor-ESPRIT.

[2] It is also possible to construct shift invariance equations from $\boldsymbol{\mathcal{V}}_q^{(\mathrm{nc},r)} = \boldsymbol{\mathcal{S}}^{(r)[\mathrm{s}]} \times_q \boldsymbol{U}_q^{(r)[\mathrm{s}]}$, however for $q \neq r$ the number of sensors is not virtually doubled and therefore $q = r$ is always a better choice.

As shown in [8], forward-backward averaging and the transformation into the real-valued domain can be formulated in terms of tensors in the following manner

$$\varphi\left(\boldsymbol{\mathcal{Z}}^{(\mathrm{nc},r)}\right) = \boldsymbol{\mathcal{Z}}^{(\mathrm{nc},r)} \times_1 \boldsymbol{Q}_{M_1}^{\mathrm{H}} \ldots \times_R \boldsymbol{Q}_{M_R}^{\mathrm{H}} \times_{R+1} \boldsymbol{Q}_{2N}^{\mathrm{H}} \tag{19}$$
$$\boldsymbol{\mathcal{Z}}^{(\mathrm{nc},r)} = \left[\boldsymbol{\mathcal{X}}^{(\mathrm{nc},r)} \sqcup_{R+1} \left(\boldsymbol{\mathcal{X}}^{(\mathrm{nc},r)^*} \times_1 \boldsymbol{\Pi}_{M_1} \ldots \times_{R+1} \boldsymbol{\Pi}_N\right)\right]$$

where $\boldsymbol{Q}_p$ represent the unitary sparse left-$\boldsymbol{\Pi}$-real matrices of size $p \times p$ introduced in [5]. Note that (19) requires a matrix $\boldsymbol{Q}_{2M_r}$ of size $2M_r \times 2M_r$ in the r-th mode. As for NC Unitary ESPRIT there is a convenient way to compute (19) directly from the measurements, since

$$\varphi\left(\boldsymbol{\mathcal{Z}}^{(\mathrm{nc},r)}\right) = \left[\left(2 \cdot \mathrm{Re}\left\{\bar{\boldsymbol{\mathcal{X}}}^{(r)}\right\} \sqcup_r 2 \cdot \mathrm{Im}\left\{\bar{\boldsymbol{\mathcal{X}}}^{(r)}\right\}\right) \sqcup_{R+1} \boldsymbol{\mathcal{O}}_{M_1 \times \ldots \times 2M_r \times \ldots \times M_R \times N}\right], \text{ where}$$
$$\bar{\boldsymbol{\mathcal{X}}}^{(r)} = \boldsymbol{\mathcal{X}} \times_1 \boldsymbol{Q}_{M_1}^{\mathrm{H}} \ldots \times_{r-1} \boldsymbol{Q}_{M_{r-1}}^{\mathrm{H}} \times_{r+1} \boldsymbol{Q}_{M_{r+1}}^{\mathrm{H}} \ldots \times_R \boldsymbol{Q}_{M_R}^{\mathrm{H}}$$

and $\boldsymbol{\mathcal{O}}$ represents the zero tensor. Let the real-valued HOSVD of $\varphi\left(\boldsymbol{\mathcal{Z}}^{(\mathrm{nc},r)}\right)$ be given by (the last N slices in the $(R+1)$-th mode can be dropped prior to computing the HOSVD)

$$\varphi\left(\boldsymbol{\mathcal{Z}}^{(\mathrm{nc},r)}\right) = \boldsymbol{\mathcal{L}}^{(r)[\mathrm{s}]} \times_1 \boldsymbol{E}_1^{(r)[\mathrm{s}]} \ldots \times_R \boldsymbol{E}_R^{(r)[\mathrm{s}]} \times_{R+1} \boldsymbol{E}_{R+1}^{(r)[\mathrm{s}]}. \tag{20}$$

We can then express the real-valued equivalent of (16) in the following fashion

$$\boldsymbol{\mathcal{F}}_r^{(\mathrm{nc},r)} \times_r \boldsymbol{K}_1^{(\mathrm{nc})(r)} \times_{R+1} \boldsymbol{\Upsilon}^{(r)} = \boldsymbol{\mathcal{F}}_r^{(\mathrm{nc},r)} \times_r \boldsymbol{K}_2^{(\mathrm{nc})(r)},$$
$$\text{where } \boldsymbol{\mathcal{F}}_r^{(\mathrm{nc},r)} = \boldsymbol{\mathcal{L}}^{(r)[\mathrm{s}]} \times_r \boldsymbol{E}_r^{(r)[\mathrm{s}]}, \tag{21}$$

and the transformed selection matrices are given by

$$\boldsymbol{K}_1^{(\mathrm{nc})(r)} = 2 \cdot \mathrm{Re}\left\{\boldsymbol{Q}_{2M_r^{(\mathrm{sel})}}^{\mathrm{H}} \cdot \boldsymbol{J}_2^{(\mathrm{nc})(r)} \cdot \boldsymbol{Q}_{2M_r}\right\} \tag{22}$$
$$\boldsymbol{K}_2^{(\mathrm{nc})(r)} = 2 \cdot \mathrm{Im}\left\{\boldsymbol{Q}_{2M_r^{(\mathrm{sel})}}^{\mathrm{H}} \cdot \boldsymbol{J}_2^{(\mathrm{nc})(r)} \cdot \boldsymbol{Q}_{2M_r}\right\}. \tag{23}$$

The matrices $\boldsymbol{\Upsilon}^{(r)}$ are estimated from (21) by an appropriate least squares method (e.g., LS, SLS [4] or TS-SLS [10]). To achieve automatic pairing of the spatial frequencies across dimensions, the eigenvalues of $\boldsymbol{\Upsilon}^{(r)}$ are estimated jointly for all $r = 1, 2, \ldots, R$. This can be accomplished by a simultaneous Schur decomposition [6] or by simultaneous diagonalization, since in the absence of noise, the matrices satisfy $\boldsymbol{\Upsilon}^{(r)} = \boldsymbol{T} \cdot \boldsymbol{\Omega}^{(r)} \cdot \boldsymbol{T}^{-1}$, where $\boldsymbol{\Omega}^{(r)}$ is a diagonal matrix with the terms $\omega_i^{(r)}$ on its diagonal for $i = 1, 2, \ldots, d$. In other words even though the matrices $\boldsymbol{\Upsilon}^{(r)}$ stem from different HOSVDs of the individual augmented measurement tensors, they share same transform matrix $\boldsymbol{T}$, which facilitates the pairing. This can be shown using the fact that in the absence of noise $\boldsymbol{\mathcal{A}} = \boldsymbol{\mathcal{U}}^{[\mathrm{s}]} \times_{R+1} \boldsymbol{T}$ [8]. From the estimated $\omega_i^{(r)}$, the spatial frequencies are obtained using the relation $\mu_i^{(r)} = 2 \arctan\left(\omega_i^{(r)}\right)$ [6].

6. SIMULATION RESULTS

To demonstrate the superior performance of NC R-D Unitary Tensor-ESPRIT compared to previous approaches, we present some numerical simulations in this section. Here, we compare 2-D versions of Unitary ESPRIT (UE) [5], Unitary Tensor-ESPRIT (UTE) [8], NC Unitary ESPRIT (NC UE) [7], and the NC Unitary Tensor-ESPRIT algorithm (NC UTE) proposed in this paper. For the first two algorithms, the corresponding deterministic Cramér-Rao bound [12] is shown, for the latter two we plot the deterministic Cramér-Rao bound for strict-sense non-circular sources (CRBnc) [9] as a

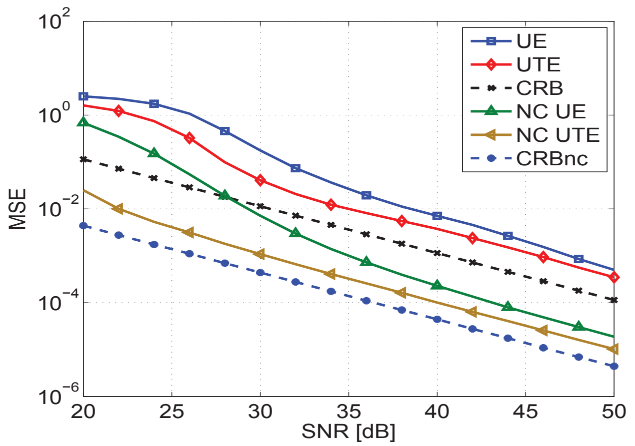

Fig. 1. Mean square estimation error (summed over sources and modes) versus signal to noise ratio for a scenario with $d = 3$ correlated sources ($\rho = 0.99$) at fixed positions $\mu_1^{(1)} = \mu_1^{(2)} = 1, \mu_2^{(1)} = \mu_2^{(2)} = 0.85, \mu_3^{(1)} = \mu_3^{(2)} = 1.15$ emitting Gaussian distributed symbols with phase angles $\varphi_1 = 0, \varphi_2 = \pi/2, \varphi_3 = \pi/4$ radiating towards a 5×7 URA which collects $N = 10$ snapshots in time.

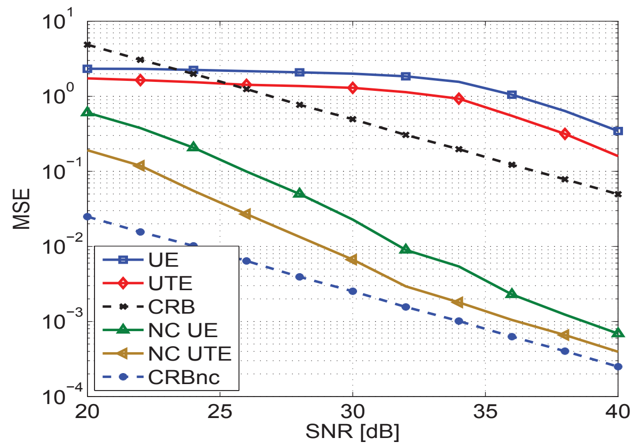

Fig. 2. Mean square estimation error (summed over sources and modes) versus signal to noise ratio for a 6×6 array capturing $N = 10$ snapshots from $d = 4$ uncorrelated sources at fixed positions $\mu_1^{(1)} = \mu_1^{(2)} = 1, \mu_2^{(1)} = \mu_2^{(2)} = 0.9, \mu_3^{(1)} = \mu_3^{(2)} = 0.8, \mu_4^{(1)} = \mu_4^{(2)} = 0.7$ emitting Gaussian distributed symbols with phase angles $\varphi_1 = 0, \varphi_2 = \pi/6, \varphi_3 = \pi/3, \varphi_4 = \pi/2$.

comparison. The mean squared errors are obtained via Monte Carlo simulations averaged over 2000 experiments.

The simulation results depicted in Fig. 1 show a scenario where a 5×7 uniform rectangular array (URA) captures $N = 10$ temporal snapshots of $d = 3$ sources at the fixed positions $\mu_1^{(1)} = \mu_1^{(2)} = 1, \mu_2^{(1)} = \mu_2^{(2)} = 0.85, \mu_3^{(1)} = \mu_3^{(2)} = 1.15$. The matrix $\boldsymbol{S}_0$ in (3) contains real-valued Gaussian distributed symbols, the sources are correlated with a pairwise correlation of $\rho = 0.99$, and have fixed phase angles of $\varphi_1 = 0, \varphi_2 = \pi/2, \varphi_3 = \pi/4$. We observe that Unitary Tensor-ESPRIT and NC Unitary ESPRIT outperform Unitary ESPRIT and that NC 2-D Unitary Tensor-ESPRIT has an even better accuracy since it can benefit of non-circular sources and the 2-D structure at the same time.

Similarly, Fig. 2 demonstrates the superiority of the novel algorithm in a scenario where $d = 4$ uncorrelated sources with real-valued Gaussian distributed symbols in $\boldsymbol{S}_0$ are considered and an 8×8 URA with $N = 10$ snapshots is used. For this scenario, the positions of the sources are given by $\mu_1^{(1)} = \mu_1^{(2)} = 1, \mu_2^{(1)} = \mu_2^{(2)} = 0.9, \mu_3^{(1)} = \mu_3^{(2)} = 0.8, \mu_4^{(1)} = \mu_4^{(2)} = 0.7$ and the phase angles are set to $\varphi_1 = 0, \varphi_2 = \pi/6, \varphi_3 = \pi/3, \varphi_4 = \pi/2$.

7. CONCLUSIONS

In this paper we propose the novel efficient direction-of-arrival estimation algorithm NC R-D Unitary Tensor-ESPRIT. Similarly to R-D Unitary Tensor-ESPRIT it is based on the HOSVD and therefore it exploits the R-dimensional structure of the measured data already in the subspace estimation step. Moreover, we show that the non-circularity of the source symbols can very effectively be exploited in the tensor case. The "virtual doubling" of the available sensors that was proposed for NC Unitary ESPRIT cannot be used in the tensor case because the augmented measurement matrix does not have an equivalent tensor form. However, we show that the augmentation can be applied in all R dimensions separately and then joined via a modified version of the tensor shift invariance equations. Therefore, all R shift invariance equations in an R-D harmonic retrieval problem are affected. Simulation results show that NC R-D Unitary Tensor-ESPRIT outperforms NC Unitary ESPRIT and R-D Unitary Tensor-ESPRIT significantly.

REFERENCES

[1] P. Chargé, Y. Wang, and J. Saillard, "A non circular sources direction finding method using polynomial rooting", *Signal Processing*, vol. 81, pp. 1765–1770, 2001.

[2] L. de Lathauwer, B. de Moor, and J. Vanderwalle, "A multilinear singular value decomposition", *SIAM J. Matrix Anal. Appl.*, vol. 21, no. 4, 2000.

[3] J. P. Delmas, "Asymptotically minimum variance second-order estimation for non-circular signals with application to DOA estimation", *IEEE Transactions on Signal Processing*, vol. 52, pp. 1235–1241, May 2004.

[4] M. Haardt, "Structured least squares to improve the performance of ESPRIT-type algorithms", *IEEE Transactions on Signal Processing*, vol. 45(3), pp. 792–799, Mar. 1997.

[5] M. Haardt and J. A. Nossek, "Unitary ESPRIT: How to obtain increased estimation accuracy with a reduced computational burden", *IEEE Trans. Signal Processing*, vol. 43, pp. 1232–1242, 1995.

[6] M. Haardt and J. A. Nossek, "Simultaneous Schur decomposition of several nonsymmetric matrices to achieve automatic pairing in multidimensional harmonic retrieval problems", *IEEE Transactions on Signal Processing*, vol. 46, pp. 161–169, Jan. 1998.

[7] M. Haardt and F. Roemer, "Enhancements of Unitary ESPRIT for non-circular sources", in *Proc. IEEE International Conference on Acoustics, Speech and Signal Processing (ICASSP 2004)*, vol. 2, pp. 101–104, Montreal, Canada, May 2004.

[8] M. Haardt, F. Roemer, and G. Del Galdo, "Higher-order SVD based subspace estimation to improve the parameter estimation accuracy in multi-dimensional harmonic retrieval problems", *IEEE Transactions on Signal Processing*, vol. 56, pp. 3198–3213, July 2008.

[9] F. Roemer and M. Haardt, "Deterministic Cramér-Rao Bounds for strict sense non-circular sources", in *Proc. International ITG/IEEE Workshop on Smart Antennas (WSA'07)*, Vienna, Austria, Feb. 2007.

[10] F. Roemer and M. Haardt, "Tensor-structure structured least squares (TS-SLS) to improve the performance of multi-dimensional ESPRIT-type algorithms", in *Proc. IEEE International Conference on Acoustics, Speech and Signal Processing (ICASSP 2007)*, vol. II, pp. 893–896, Honolulu, HI, Apr. 2007.

[11] A. Salameh, N. Tayem, and H. M. Kwon, "Improved 2-D Root MUSIC for Non-Circular Signals", in *Fourth IEEE Workshop on Sensor Array and Multichannel Processing*, pp. 151–156, July 2006.

[12] P. Stoica and A. Nehorai, "MUSIC, maximum likelihood, and Cramer-Rao bound", *IEEE Transactions on Acoustics, Speech, and Signal Processing*, vol. 37, pp. 720–741, May 1989.

[13] A. Zoubir, P. Chargé, and Y. Wang, "Non circular sources localization with ESPRIT", in *Proc. European Conference on Wireless Technology (ECWT 2003)*, Munich, Germany, Oct. 2003.